Comput Mech (2011) 48:713–727
DOI 10.1007/s00466-011-0616-3

ORIGINAL PAPER

An inelastic Timoshenko beam element with axial–shear–flexural interaction

Savvas P. Triantafyllou · Vlasis K. Koumousis

Received: 14 August 2010 / Accepted: 6 June 2011 / Published online: 28 June 2011

Abstract An enhanced beam element is proposed for the nonlinear dynamic analysis of skeletal structures. The formulation extends the displacement based elastic Timoshenko beam element. Shear-locking effects are eliminated using exact shape functions. A variant of the Bouc–Wen model is implemented to incorporate plasticity due to combined axial, shear and bending deformation components. Interaction is introduced through the implementation of yield functions, expressed in the stress resultant space. Three additional hysteretic degrees of freedom are introduced to account for the hysteretic part of the deformation components. Numerical results are presented that demonstrate the advantages of the proposed element in simulating cyclic phenomena, in which shear deformations are significant.

Keywords Timoshenko beam · Hysteretic model · Bouc–Wen · Finite elements

1 Introduction

Modern design codes allow structures to undergo significant inelastic deformations prior to collapse. Furthermore, excessive dynamical loading, away from code specified design levels, stresses the structure to ultimate states underlining the need for the simulation of nonlinear response due to material nonlinearities. In this context, various beam elements have been proposed either through displacement based formulations [4] or force based formulations [35]. Material nonlinearity is introduced at the section level, either macroscopically through a plastic-hinge approach [20] or through a fibre-based formulation at the element level [25,32]. In the former, the Timoshenko beam theory is implemented within the framework of a force based distributed plasticity formulation. Although more accurate, the fibre based formulation comes at the cost of requiring numerical integrations at the section level. At least three points of integration are needed to achieve a linear distribution of the curvature along the element's length with the most efficient Lobatto rule [35]. Thus, in a time marching-process as a nonlinear dynamic analysis, the computational advantage of concentrated plasticity, displacement based schemes remains significant.

The Timoshenko beam theory has not been addressed in such problems, mainly due to the shear locking problem [28,37] of the displacement based isoparametric formulation that can lead to inaccurate results both in the linear and nonlinear case. The Timoshenko beam theory leads to increased structural displacements. This increase can be even greater under dynamical excitation since the dynamic characteristics of the structure are altered. Such deviations from the standard Euler–Bernoulli based approach can have significant influence on the displacement based design of structures [1]. In structural members that are subjected to high shear forces, as in shear links of eccentrically braced frames, shear effects are very important both in the elastic and inelastic regime [17].

So far, considerable effort has been made in introducing the Bouc–Wen model into the inelastic analysis of skeletal structures and structural joints [10]. In [12], a force based concentrated plasticity beam element is derived, within the framework of Euler–Bernoulli assumption, that accounts only for plastic bending deformations. Symeonov et al. [38] introduce an Euler–Bernoulli, force based, element

S. P. Triantafyllou · V. K. Koumousis (✉)
Institute of Structural Analysis and Aseismic Research,
National Technical University of Athens, Zografou Campus,
15780 Athens, Greece
e-mail: vkoum@central.ntua.gr

S. P. Triantafyllou
e-mail: savtri@central.ntua.gr

formulation where interaction between the axial force and the bending moment is considered. This formulation leads to a non-constant flexibility matrix which depends on both the moment and the curvature of a given cross-section. Although exact, especially in the case of members of variable cross-sections, this approach leads to an increased computational cost due to the fact that state matrices do not remain constant and need updating, as the solution evolves.

When studying the dynamic behaviour of nonlinear systems, dissipation phenomena are of the utmost importance. As such, hysteretic damping needs to be addressed directly by incorporating a hysteretic rule to model the cyclic response of the structure. One such attempt was initiated by Bouc in his original formulation of the single degree degrading hysteresis model [5], followed by several modifications introduced, such as the Bouc–Wen model [42], the Baber–Noori model [3] and the Reinhorn model [34]. These models of hysteresis—also known as smooth hysteretic models—are capable of simulating a number of different types of hysteretic response using a single smooth hysteretic function. The advantages of the Bouc–Wen model as compared to other rate independent hysteretic models, either smooth such as the Ozdemir model [24] and the Ramberg–Osgood model [29] or piece-wise linear such as the Takeda model and the Q-hyst model [31], have been extensively reviewed in the literature [15].

In this work, a displacement based beam element is proposed for the nonlinear dynamic analysis of skeletal structures. Inelasticity is introduced at a macro-level, considering three additional degrees of freedom, namely the hysteretic axial deformation, the hysteretic shear deformation and the hysteretic curvature. These additional degrees of freedom are set to evolve according to the Bouc–Wen hysteresis model. Moreover, different hysteretic parameters can be attributed at each end, yielding a versatile formulation for e.g. steel members bearing different connections in each end. Using the variational principle of virtual work, a modified hysteretic stiffness matrix is derived that can be easily incorporated into existing finite element schemes within the framework of the direct stiffness method. Alternatively, an advanced customized solution procedure may be implemented. In this, the governing equations of the problem are formulated in state-space form and the solution is obtained using a predictor–corrector differential equation solver that results in solutions of improved accuracy.

The present work is structured as follows: In Sect. 2, the properties of the implemented Bouc–Wen hysteretic rule are introduced. In Sect. 3, the formulation of the element is presented. For the sake of clarity, only the planar case is examined in this work, whereas the 3D beam element formulation can be derived in a straightforward similar manner. Six new, hysteretic degrees of freedom are defined (three per node) which follow the Bouc–Wen hysteretic rule. The proposed solution algorithm is then described in Sect. 4. Finally, numerical examples are presented which demonstrate the robustness of the method in terms of accuracy and computational speed.

2 The Bouc–Wen hysteretic model

2.1 The multi-axial formulation of Bouc–Wen hysteresis

The Bouc–Wen model was introduced by Bouc [5] and modified subsequently by Wen [42], Baber and Noori [3] and Reinhorn [34]. To account for yield criteria involving more than one components of the stress tensor, a general formulation is needed to address the inherent interaction. Following Sivaselvan and Reinhorn [35] the stress tensor can be decomposed into an elastic and hysteretic part as follows:

$$\{\sigma\}=\left\{\sigma^{e}\right\}+\{\sigma^{h}\}=[\alpha]\,[E]\,\{\varepsilon\}+([I]-[\alpha])\,[E]\,\{z\} \tag{1}$$

where $\{\sigma\}$ is the 6×1 stress vector, $\{\sigma^{e}\}$ is considered the elastic part of the stress tensor, $\{\sigma^{h}\}$ the hysteretic part of the stress tensor, $[\alpha]$ denotes a square diagonal matrix with post yield to elastic stiffness moduli, $[E]$ is the elastic constitutive matrix [13], $[I]$ is the identity matrix, $\{\varepsilon\}$ is the 6×1 strain vector and $\{z\}$ is a 6×1 hysteretic strain vector. A hysteretic 6×1 stress vector is thus defined as:

$$\{\sigma^{h}\}=\left[E^{h}\right]\{z\} \tag{2}$$

where

$$\left[E^{h}\right]=([I]-[\alpha])\,[E] \tag{3}$$

Casciati [6] proves that if the hysteretic vector evolves according to the following Bouc–Wen hysteretic rule:

$$\{\dot{\sigma}^{h}\}=\left[E^{h}\right]\{\dot{z}\}=\left[E^{h}\right]([I]-H_1H_2\,[R])\,\{\dot{\varepsilon}\} \tag{4}$$

then Eq. 1 accurately describes the nonlinear hysteretic behaviour of a material with linear kinematic hardening in the 3D stress space. In relation (4) H_1 and H_2 are smoothed Heaviside functions expressed in the following form:

$$\begin{aligned} H_1&=\left\|\Phi\left(\left\{\sigma^{h}\right\}\right)+1\right\|^{n}\\ H_2&=\gamma\,\mathrm{sgn}\left(\left\{\sigma^{h}\right\}^{T}\{\dot{\varepsilon}\}\right)+\beta \end{aligned} \tag{5}$$

where $\Phi\left(\{\sigma^{h}\}\right)$ is a yield criterion such that:

$$\Phi\left(\{\sigma^{h}\}\right)-1\leq0 \tag{6}$$

with the equality holding when yield has occurred. In Eq. 5 n is the smoothing parameter and β, γ are shape factors that define the shape of the loading and unloading branches of the hysteretic loop. The first of Eq. 5 smooths the transition from the elastic to the inelastic region. The second controls the

unloading phases under cyclic excitation. Equations 1–6 can be alternatively formulated in the stress-resultant space considering the proper, elastic, constitutive matrix and the proper vector of strains conjugate to the stress-resultants [38].

Since rates of the corresponding parameters appear in both sides of Eq. 4 the hysteretic vector $\{z\}$ is rate independent. The typical elastic-perfectly plastic hysteretic behaviour can be derived, setting $\beta = \gamma = 0.5$, $n > 6$ in Eq. (5) and $[\alpha] = \emptyset$ in Eq. 1, while a variety of other responses can also be obtained [34].

Matrix [R] in relation (4) is an interaction matrix that depends on the yield function, given as:

$$[R] = \left[\left(\frac{\partial \Phi}{\partial \{\sigma^h\}}\right)^T [E] \left(\frac{\partial \Phi}{\partial \{\sigma^h\}}\right)\right]^{-1} \times \left[\left(\frac{\partial \Phi}{\partial \{\sigma^h\}}\right)\left(\frac{\partial \Phi}{\partial \{\sigma^h\}}\right)^T [E]\right] \tag{7}$$

The interaction matrix $[R]$ is formally derived by taking into account the consistency condition of associative plasticity [6]. Equations 1 and 4, yield a versatile formulation within the classical plasticity framework, where most of the associative flow rules are expressed in the stress space [18].

3 Beam element formulation

3.1 Kinematic relations

A typical element of length L is considered (Fig. 1) in which the nodal degrees of freedom in the local coordinate system are:

$$\{d\} = \{u_1 \; w_1 \; \theta_1 \; u_2 \; w_2 \; \theta_2\}^T \tag{8}$$

The following kinematic assumptions are considered according to the Timoshenko theory of bending, i.e. plane sections remain plane but not necessarily normal to the neutral axis (Fig. 2):

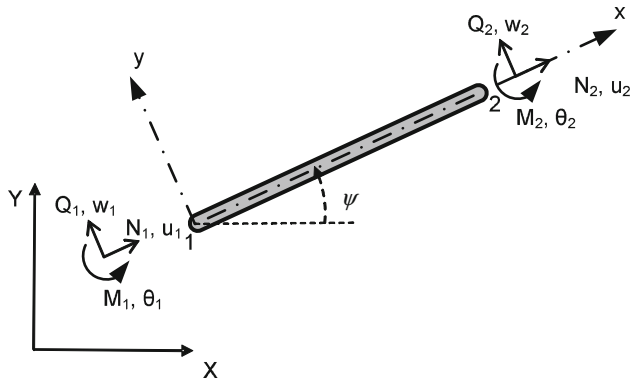

Fig. 1 Nodal displacements and loads

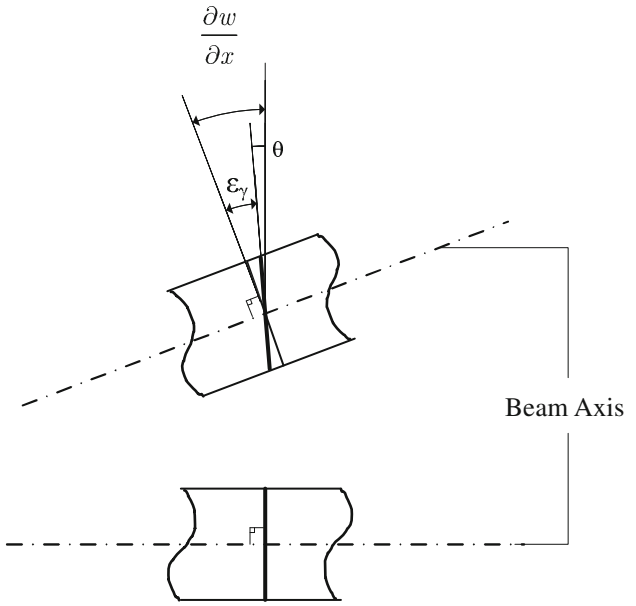

Fig. 2 Timoshenko kinematic assumption

$$\varepsilon_u = \frac{\partial u}{\partial x}, \quad \varepsilon_\phi = \frac{\partial \theta}{\partial x}, \quad \varepsilon_\gamma = \frac{\partial w}{\partial x} - \theta \tag{9}$$

3.2 Exact shape functions

In the work presented herein, the shape functions implemented are explicitly derived from the exact solution of the homogeneous Timoshenko beam differential equations as proposed in [28] and [11]. The Timoshenko beam differential equations are defined as:

$$\begin{cases} EI\frac{\partial^2 \theta}{\partial x^2} + kGA\left(\frac{\partial w}{\partial x} - \theta\right) = 0 \\ kGA\left(\frac{\partial^2 w}{\partial x^2} - \frac{\partial \theta}{\partial x}\right) = 0 \end{cases} \tag{10}$$

where EI is the flexural rigidity of the cross-section, GA is the shear rigidity of the cross-section and k is the shear correction coefficient of the cross-section [9]. Solving Eq. (10) as proposed in [11] the following interpolation field is derived, including also the axial displacements:

$$\begin{aligned} u(x) &= N_1 u_1 + N_4 u_2 \\ w(x) &= N_2 w_1 + N_3 \theta_1 + N_5 w_2 + N_6 \theta_2 \\ \theta(x) &= N_7 w_1 + N_8 \theta_1 + N_9 w_2 + N_{10} \theta_2 \end{aligned} \tag{11}$$

where the interpolation functions N_i introduced in Eq. 11 assume the following form:

$$
\begin{aligned}
N_1 &= 1-\tfrac{x}{L}\\
N_2 &= \tfrac{2\mu}{L^3}x^3-\tfrac{3\mu}{L^2}x^2-\tfrac{12\lambda\mu}{L}x+1\\
N_3 &= \tfrac{\mu}{L^2}x^3-\tfrac{2(1+3\lambda)\mu}{L}x^2+(6\lambda+1)\,\mu x\\
N_4 &= \tfrac{x}{L}\\
N_5 &= -\tfrac{2\mu}{L^3}x^3+\tfrac{3\mu}{L^2}x^2+\tfrac{12\lambda\mu}{L}x\\
N_6 &= \tfrac{\mu}{L^2}x^3-\tfrac{(-6\lambda+1)\mu}{L}x^2-6\lambda\mu x\\
N_7 &= \tfrac{6\mu}{L^3}x^2-\tfrac{6\mu}{L^2}x\\
N_8 &= \tfrac{3\mu}{L^2}x^2-\tfrac{4(1+3\lambda)\mu}{L}x+\mu\,(12\lambda+1)\\
N_9 &= -\tfrac{6\mu}{L^3}x^2+\tfrac{6\mu}{L^2}x\\
N_{10} &= \tfrac{3\mu}{L^2}x^2-\tfrac{2\mu(1-6\lambda)}{L}x
\end{aligned}
\tag{12}
$$

with:

$$
\mu=\frac{1}{1+12\lambda},\quad \lambda=\frac{EI}{kGAL^2} \tag{13}
$$

The stiffness matrix of the element is then derived following the standard procedure of the Finite Element Method, [4], as:

$$
K=\frac{EI}{L^3}\begin{bmatrix}
\frac{L^2A}{I} & 0 & 0 & -\frac{L^2A}{I} & 0 & 0\\
0 & 12\mu & 6\mu L & 0 & -12\mu & 6\mu L\\
0 & 6\mu L & 4\mu\,(1+3\lambda)\,L^2 & 0 & -6\mu L & 2\mu\,(1-6\lambda)\,L^2\\
-\frac{L^2A}{I} & 0 & 0 & \frac{L^2A}{I} & 0 & 0\\
0 & -12\mu & -6\mu L & 0 & 12\mu & -6\mu L\\
0 & 6\mu L & 2\mu\,(1-6\lambda)\,L^2 & 0 & -6\mu L & 4\mu\,(1+3\lambda)\,L^2
\end{bmatrix} \tag{14}
$$

Contrary to the isoparametric finite element method, the element material properties are naturally considered in the interpolation functions through the constants λ and μ. As λ tends to zero, μ approaches unity, and the stiffness matrix of Eq. 14 degenerates into the Euler–Bernoulli stiffness matrix. The stiffness matrix is identical to the stiffness matrix of the Timoshenko beam element proposed by Macneal in [19] through the residual bending flexibility method or RBF. The approach adopted in the present work, as introduced in [11], offers an interesting alternative with a better insight on the mechanics of the locking phenomenon. Moreover, the derived stiffness matrix is identical to the one derived by the exact, force based Timoshenko beam element formulation as described in [39].

Taking into account the axial degrees of freedom the following, augmented, strain-displacement matrix is derived, which corresponds to the $6x1$ nodal displacement vector presented in relation (8):

$$
[B]=\begin{bmatrix}
-\frac{1}{L} & 0 & 0\\
0 & -\frac{12\lambda\mu}{L} & -\frac{6\mu(-2x+L)}{L^3}\\
0 & -6\lambda\mu & -\frac{2\mu}{L}\left(-3\frac{x}{L}+2\,(1+3\lambda)\right)\\
\frac{1}{L} & 0 & 0\\
0 & \frac{12\lambda\mu}{L} & \frac{6\mu(-2x+L)}{L^3}\\
0 & -6\lambda\mu & \frac{2\mu}{L}\left(3\frac{x}{L}-1+6\lambda\right)
\end{bmatrix}^T \tag{15}
$$

Throughout the work presented herein, axial and bending deformations are considered to be uncoupled as implied by the kinematic assumptions considered in Eq. 9.

3.3 The hysteretic degrees of freedom

Based on the previous results, the elastic deformation field is extended herein by introducing an additional vector of corresponding hysteretic degrees of freedom:

$$
\varepsilon=\left\{\varepsilon_u\ \varepsilon_\gamma\ \varepsilon_\phi\right\}^T\rightarrow\tilde{\varepsilon}=\left\{\{\varepsilon\}\ \{z\}\right\}^T=\left\{\varepsilon_u\ \varepsilon_\gamma\ \varepsilon_\phi\ z_u\ z_\gamma\ z_\phi\right\}^T \tag{16}
$$

In Eq. 16, the elastic strain vector ε, consisting of the centreline axial deformation ε_u, the shear deformation ε_γ and the curvature ε_ϕ, is extended to its generalized counterpart $\tilde{\varepsilon}$ comprising of the total strain vector $\{\varepsilon\}$ and the hysteretic strain vector $\{z\}$. In the latter, z_u stands for the hysteretic part of the total centreline axial deformation, z_γ is the hysteretic part of the total shear strain and z_ϕ is the hysteretic part of the total curvature. The following nonlinear hysteretic laws are considered for the stress resultants:

$$
\begin{aligned}
N(x) &= \alpha_u EA\varepsilon_u(x)+(1-\alpha_u)\,EAz_u(x)\\
Q(x) &= \alpha_\gamma GA_s\varepsilon_\gamma(x)+\left(1-\alpha_\gamma\right)GA_sz_\gamma(x),\quad A_s=kA\\
M(x) &= \alpha_\phi EI\varepsilon_\phi(x)+\left(1-\alpha_\phi\right)EIz_\phi(x)
\end{aligned}
\tag{17}
$$

where $\alpha_u,\alpha_\gamma,\alpha_\phi$ are the axial, shear and bending inelastic to elastic stiffness ratios respectively. If $\alpha_i=0,\ i=u,\gamma,\phi$ then the corresponding nonlinear relation assumes an elastic perfectly plastic behaviour. If $\alpha_i=1$ then the corresponding behaviour is purely elastic. According to the generalized hysteretic formulation presented in Sect. 2.1, relation (17) can be cast in matrix form as:

$$
\begin{Bmatrix}N\\Q\\M\end{Bmatrix}_{(x)}=\begin{Bmatrix}N^e\\Q^e\\M^e\end{Bmatrix}_{(x)}+\begin{Bmatrix}N^h\\Q^h\\M^h\end{Bmatrix}_{(x)} \tag{18}
$$

where the elastic part is expressed as:

$$
\begin{Bmatrix}N^e\\Q^e\\M^e\end{Bmatrix}_{(x)}=[D]\begin{Bmatrix}\varepsilon_u\\\varepsilon_\gamma\\\varepsilon_\phi\end{Bmatrix}_{(x)} \tag{19}
$$

and the hysteretic part is derived accordingly:

$$\begin{Bmatrix} N^h \\ Q^h \\ M^h \end{Bmatrix}_{(x)} = \left[D^h\right] \begin{Bmatrix} z_u \\ z_\gamma \\ z_\phi \end{Bmatrix}_{(x)} \tag{20}$$

where (x) denotes dependence on the space variable. Matrix $[D]$ in Eq. 19 is defined as

$$[D] = \begin{bmatrix} \alpha_u EA & & \\ & \alpha_\gamma GA_s & \\ & & \alpha_\phi EI \end{bmatrix} \tag{21}$$

while matrix $\left[D^h\right]$ in Eq. 20 is defined as

$$\left[D^h\right] = \begin{bmatrix} (1-\alpha_u)\, EA & & \\ & \left(1-\alpha_\gamma\right) GA_s & \\ & & \left(1-\alpha_\phi\right) EI \end{bmatrix} \tag{22}$$

The evolution equations of the hysteretic components are defined in the form of Eq. 4 as follows:

$$\begin{aligned} \begin{Bmatrix} \dot{N}^h \\ \dot{Q}^h \\ \dot{M}^h \end{Bmatrix}_{(x)} &= \left[D^h\right] \begin{Bmatrix} \dot{z}_u \\ \dot{z}_\gamma \\ \dot{z}_\phi \end{Bmatrix}_{(x)} \\ &= \left[D^h\right] \left([I] - H_1 H_2 [R]\right) \begin{Bmatrix} \dot{\varepsilon}_u \\ \dot{\varepsilon}_\gamma \\ \dot{\varepsilon}_\phi \end{Bmatrix}_{(x)} \end{aligned} \tag{23}$$

Equation 23 is expressed in terms of hysteretic deformations as:

$$\begin{Bmatrix} \dot{z}_u \\ \dot{z}_\gamma \\ \dot{z}_\phi \end{Bmatrix}_{(x)} = \left([I] - H_1 H_2 [R]\right) \begin{Bmatrix} \dot{\varepsilon}_u \\ \dot{\varepsilon}_\gamma \\ \dot{\varepsilon}_\phi \end{Bmatrix}_{(x)} \tag{24}$$

where according to Eq. 5 H_1, H_2 may assume the following form:

$$\begin{aligned} H_1 &= \left\| \Phi\left(\left\{N^h \;\; Q^h \;\; M^h\right\}^T\right) + 1 \right\|^n, \qquad n \geq 2 \\ H_2 &= \gamma \mathrm{sgn}\left(\left\{N^h \;\; Q^h \;\; M^h\right\}^T \begin{Bmatrix} \dot{\varepsilon}_u \\ \dot{\varepsilon}_\gamma \\ \dot{\varepsilon}_\phi \end{Bmatrix} \right) + \beta \end{aligned} \tag{25}$$

The yield surface Φ is expressed as a function of the hysteretic parts of the stress resultants defined in Eq. 20.

Furthermore, the interaction matrix $[R]$ is now expressed with respect to a stress-resultant based interaction surface as:

$$\begin{aligned} [R] = &\left[\left(\frac{\partial \Phi}{\partial \left\{P^h\right\}} \right)^T [D] \left(\frac{\partial \Phi}{\partial \left\{P^h\right\}} \right) \right]^{-1} \\ &\times \left[\left(\frac{\partial \Phi}{\partial \left\{P^h\right\}} \right) \left(\frac{\partial \Phi}{\partial \left\{P^h\right\}} \right)^T [D] \right] \end{aligned} \tag{26}$$

where $\left\{P^h\right\}_{(x)} = \left\{N^h \;\; Q^h \;\; M^h\right\}^T_{(x)}$.

The definition of the yield surface Φ depends on the geometric properties of the cross-section under consideration. Different formulations exist for rectangular, hollow and I-shaped, concrete or steel sections such as the Hodge's scheme [18] and the general yield function proposed by Neal in [22]. The yield surface can also be derived numerically on the grounds of a fiber analysis [7]. In this case, relation (26) is also evaluated numerically. In the example Section of this work several yield surface formulations are presented.

Usually the nonlinear interaction between moment and shear is considered to be negligible, contrary to the axial–moment interaction. In this case, relation (23) is reformulated, to account for coupled axial–moment and uncoupled shear plasticity patterns as follows:

$$\begin{aligned} \begin{Bmatrix} \dot{N}^h \\ \dot{M}^h \end{Bmatrix}_{(x)} &= \begin{bmatrix} (1-\alpha_u)\, EA & \\ & \left(1-\alpha_\phi\right) EI \end{bmatrix} \begin{Bmatrix} \dot{z}_u \\ \dot{z}_\phi \end{Bmatrix}_{(x)} \\ &= \begin{bmatrix} (1-\alpha_u)\, EA & \\ & \left(1-\alpha_\phi\right) EI \end{bmatrix} \left([I] - H_1 H_2 [R]\right) \begin{Bmatrix} \dot{\varepsilon}_u \\ \dot{\varepsilon}_\phi \end{Bmatrix}_{(x)} \\ \dot{Q}^h &= \left(1-\alpha_\gamma\right) GA_s \dot{z}_\gamma = \left(1-\alpha_\gamma\right) GA_s \left(1 - H_1^s H_2^s\right) \dot{\varepsilon}_\gamma \end{aligned} \tag{27}$$

or:

$$\begin{Bmatrix} \dot{z}_u \\ \dot{z}_\phi \\ \dot{z}_\gamma \end{Bmatrix}_{(x)} = \begin{bmatrix} [I] - H_1 H_2 [R] & \begin{matrix} 0 \\ 0 \end{matrix} \\ \begin{matrix} 0 & 0 \end{matrix} & \left(1 - H_1^s H_2^s\right) \end{bmatrix} \begin{Bmatrix} \dot{\varepsilon}_u \\ \dot{\varepsilon}_\phi \\ \dot{\varepsilon}_\gamma \end{Bmatrix}_{(x)} \tag{28}$$

where in the first of Eq. 27 H_1, H_2 and $[R]$, are functions of the hysteretic axial force and the hysteretic moment. In the second of Eq. 27:

$$H_1^s = \left| \frac{Q^h}{Q_y^h} \right|^n, \qquad H_2^s = \beta_s + \gamma_s \mathrm{sgn}\left(Q^h \dot{\varepsilon}_\gamma\right) \tag{29}$$

and $Q_y^h = \left(1-\alpha_\gamma\right) Q_y$ is the hysteretic yield shear force, while Q_y is the yield force of the cross-section in shear.

3.4 Additional shape functions

Based on the deformation vector defined in Eq. 16, the vector of nodal degrees of freedom introduced in Section 3.1 is herein extended to the 12×1 vector $\left\{\tilde{d}\right\}$

$$\left\{\tilde{d}\right\} = \left\{\{d\} \; \{z\}\right\} = \left\{u_1 \;\; w_1 \;\; \theta_1 \;\; u_2 \;\; w_2 \;\; \theta_2 \;\; z_u^1 \;\; z_u^2 \;\; z_\gamma^1 \;\; z_\gamma^2 \;\; z_\phi^1 \;\; z_\phi^2\right\}^T \tag{30}$$

which consists of the total displacement vector $\{d\}$ and the hysteretic part of the total deformation $\{z\}$.

Equation 17 are rewritten in the following equivalent form:

$$N(x) = EA\left(\alpha_u \varepsilon_u(x) + (1-\alpha_u) z_u(x)\right) = EA\tilde{\varepsilon}_u(x) \tag{31}$$

$$Q(x) = GA_s\left(\alpha_\gamma \varepsilon_\gamma(x) + \left(1-\alpha_\gamma\right) z_\gamma(x)\right) = GA_s\tilde{\varepsilon}_\gamma(x) \tag{32}$$

$$M(x) = EI\left(\alpha_\phi \varepsilon_\phi(x) + \left(1-\alpha_\phi\right) z_\phi(x)\right) = EI\tilde{\varepsilon}_\phi(x) \tag{33}$$

where $\tilde{\varepsilon}_u(x)$, $\tilde{\varepsilon}_\gamma(x)$ and $\tilde{\varepsilon}_\phi(x)$ can be considered as a measure of equivalent generalized centerline axial deformation, shear deformation and curvature respectively.

The total part of the deformation component $\{\varepsilon\}$ depends solely on the total part of the displacement field as implied by the compatibility relations introduced in Eq. 9. Thus, the shape functions introduced in Eq. 12 are also used in the nonlinear case for the interpolation of the total displacement component $\{d\}$.

The definition of the hysteretic shape functions is explicitly derived from the equilibrium of the corresponding stress resultants. Since the total moments at the ends of the element are in equilibrium and there is no lateral intermediate loading the following, equilibrium based, relations hold:

$$N(x) = \xi_N N_1 + (1-\xi_N) N_2 \tag{34}$$

$$Q(x) = \xi_Q Q_1 + (1-\xi_Q) Q_2 \tag{35}$$

$$M(x) = \left(1-\frac{x}{L}\right) M_1 + \frac{x}{L} M_2 \tag{36}$$

where N_i, Q_i, M_i, $i = 1, 2$ are the values of the stress resultants at the start and end node of the beam element respectively (Fig. 1), while $\xi_i \in \left[0\ 1\right]$, $i = N, Q$.

Since the proposed element is a constant axial and shear force element, any value of ξ_i satisfies equilibrium in relations (34) and (35). Choosing $\xi_i = 1$, the axial and shear force are considered only at the end node, thus reducing the number of hysteretic degrees of freedom as proposed in [32]. However, since the proposed formulation highlights the macroscopical hysteretic properties of skeletal structures a general scheme would be preferable where different hysteretic properties can be assigned at the end nodes of each beam element. In this work the value of $\xi_i = 1/2$ is chosen that results into a symmetric interpolation scheme.

Setting $\xi_N = 1/2$ in Eq. 34 and substituting into Eq. 31 the following relation is derived:

$$\tilde{\varepsilon}_u(x) = \frac{1}{2}\frac{N_1}{EA} + \frac{1}{2}\frac{N_2}{EA} = \frac{1}{2}\tilde{\varepsilon}_u^1 + \frac{1}{2}\tilde{\varepsilon}_u^2 \tag{37}$$

Collocating the expression of the equivalent centerline axial deformation equation $\tilde{\varepsilon}_u(x)$ from relation (31) at $x = 0$ and $x = L$ the following relations are also derived from Eq. 31:

$$\tilde{\varepsilon}_u^1 = \alpha_u \varepsilon_u^1 + (1-\alpha_u) z_u^1 \tag{38}$$

and

$$\tilde{\varepsilon}_u^2 = \alpha_u \varepsilon_u^2 + (1-\alpha_u) z_u^2 \tag{39}$$

Replacing Eqs. 38 and 39 into relation (37) and performing the necessary algebraic manipulations, the following expression is obtained:

$$\alpha_u \varepsilon_u(x) + (1-\alpha_u) z_u(x) = \alpha_u\left(\frac{1}{2}\varepsilon_u^1 + \frac{1}{2}\varepsilon_u^2\right) + (1-\alpha_u)\left(\frac{1}{2}z_u^1 + \frac{1}{2}z_u^2\right) \tag{40}$$

Since relation (40) holds for every possible value of α_u the same interpolation field has to be adopted for both the total axial centerline deformation ε_u and the hysteretic axial centerline deformation z_u. Following the same procedure for the hysteretic shear deformation and the hysteretic curvature the following exact interpolation functions are finally derived:

$$z_u(x) = \left[1/2\ 1/2\right]\left\{z_u^1\ z_u^2\right\}^T$$

$$z_\gamma(x) = \left[1/2\ 1/2\right]\left\{z_\gamma^1\ z_\gamma^2\right\}^T$$

$$z_\phi(x) = \left[1-\tfrac{x}{L}\ \tfrac{x}{L}\right]\left\{z_\phi^1\ z_\phi^2\right\}^T \tag{41}$$

where z_i^j, $j = 1, 2, i = u, \gamma, \phi$ are the nodal hysteretic deformations. Thus, a hysteretic interpolation field is established denoted herein as $\left[N_z\right]$:

$$\left[N_z\right] = \begin{bmatrix} 1/2 & 1/2 & 0 & 0 & 0 & 0 \\ 0 & 0 & 1/2 & 1/2 & 0 & 0 \\ 0 & 0 & 0 & 0 & 1-\frac{x}{L} & \frac{x}{L} \end{bmatrix} \tag{42}$$

The interpolation field $\left[N_z\right]$ maps the continuous hysteretic deformation components into their corresponding nodal quantities. Accordingly, the interpolation equation is written in the following form:

$$\left\{u(x)\ w(x)\ \theta(x)\ z_u(x)\ z_\gamma(x)\ z_\phi(x)\right\}^T = \begin{bmatrix} [N] & [\emptyset] \\ [\emptyset] & [N_z] \end{bmatrix}\left\{\tilde{d}\right\} \tag{43}$$

where $[\emptyset]$ is the 3x6 null matrix. Equation 43 can be used to formulate the element's hysteretic stiffness matrix as described in the next Section.

3.5 Derivation of stiffness matrix

Taking into account bending, shear and axial deformations, the principle of virtual work is formulated as:

$$\Pi_e = \{d\}^T\{P\} = \delta V = \int_0^L \left(M\delta\varepsilon_\phi + Q\delta\varepsilon_\gamma + N\delta\varepsilon_u\right)dx \tag{44}$$

where only nodal external loads are considered for the sake of simplicity. Substituting Eq. 17 into 44 the following relation is derived:

$$\{d\}^T \{P\} = \mathscr{I}_\phi + \mathscr{I}_\gamma + \mathscr{I}_u \tag{45}$$

where

$$\mathscr{I}_\phi = \int_0^L \left(\alpha_\phi EI\varepsilon_\phi + \left(1-\alpha_\phi\right) EIz_\phi\right) \delta\varepsilon_\phi dx \tag{46}$$

$$\mathscr{I}_\gamma = \int_0^L \left(\alpha_\gamma GA_s\varepsilon_\gamma + \left(1-\alpha_\gamma\right) GA_s z_\gamma\right) \delta\varepsilon_\gamma dx \tag{47}$$

and

$$\mathscr{I}_u = \int_0^L \left(\alpha_u EA\varepsilon_u + \left(1-\alpha_u\right) EA\right) \delta\varepsilon_u dx \tag{48}$$

Collecting the hysteretic parts of the above integrals, Eq. 45 is reformulated as:

$$\begin{aligned}
&\{d\}^T \{P\} \\
&= \left(\int_0^L \left(\alpha_\phi EI\varepsilon_\phi\right) \delta\varepsilon_\phi dx \right. \\
&\quad \left. + \int_0^L \alpha_\gamma GA_s\varepsilon_\gamma \delta\varepsilon_\gamma dx + \int_0^L \alpha_u EA\varepsilon_u \delta\varepsilon_u dx \right) \\
&\quad + \left(\int_0^L \left(\left(1-\alpha_\phi\right) EIz_\phi\right) \delta\varepsilon_\phi dx + \int_0^L \left(1-\alpha_\gamma\right) GA_s z_\gamma \delta\varepsilon_\gamma dx \right. \\
&\quad \left. + \int_0^L \left(1-\alpha_u\right) EAz_u \delta\varepsilon_u dx \right)
\end{aligned} \tag{49}$$

Writing the above integrals in matrix notation and substituting for the expression of the interpolated field introduced in Eq. 43 the following relations are derived:

$$\{\delta d\}^T \{P\} = \{\delta d\}^T I_e \{\delta d\} + \{\delta d\}^T I_h \{z\} \tag{50}$$

where:

$$I_e = \int_0^L [B]^T [D][B]\, dx \tag{51}$$

and

$$I_h = \int_0^L [B]^T \left[D^h\right] \left[N_z\right] dx \tag{52}$$

where I_e is the internal energy corresponding to the total deformation components, I_h is the internal energy corresponding to the hysteretic deformation components, $[B]$ is defined in Eq. 15, $\left[N_z\right]$ in Eq. 42, $\{z\}$ is the vector of hysteretic nodal degrees of freedom and matrices $[D]$ and $\left[D^h\right]$ are defined in Eqs. 21 and 22 respectively.

Equation 51 yields the elastic stiffness matrix of the beam element:

$$[k_e] = \frac{\alpha_\phi EI}{L} \begin{bmatrix} \frac{\alpha_u EA}{\alpha_\phi EI} & 0 & 0 & -\frac{\alpha_u EA}{\alpha_\phi EI} & 0 & 0 \\ 0 & 12\Psi_3 & 6\Psi_3 & 0 & -12\Psi_3 & 6\Psi_3 \\ 0 & 6 & 4\Psi_1 & 0 & -6\Psi_3 & 2\Psi_2 \\ -\frac{\alpha_u EA}{\alpha_\phi EI} & 0 & 0 & \frac{\alpha_u EA}{\alpha_\phi EI} & 0 & 0 \\ 0 & -12\Psi_3 & -6\Psi_3 & 0 & 12\Psi_3 & -6\Psi_3 \\ 0 & 6\Psi_3 & 2\Psi_2 & 0 & -6\Psi_3 & 4\Psi_1 \end{bmatrix} \tag{53}$$

where:

$$\begin{aligned}
\Psi_1 &= \left(1 + 6\lambda + 9\frac{\alpha_\gamma}{\alpha_\phi}\lambda + 36\lambda^2\right)\mu^2 \\
\Psi_2 &= \left(1 - 12\lambda + 18\frac{\alpha_\gamma}{\alpha_\phi}\lambda - 72\lambda^2\right)\mu^2 \\
\Psi_3 &= \beta GAL\left(1 + 12\frac{\alpha_\gamma}{\alpha_\phi}\lambda\right)\mu^2
\end{aligned}$$

and λ, μ are defined in relation (13). When $\alpha_u = \alpha_\phi = \alpha_\gamma = 1$ the stiffness matrix reduces to the elastic Timoshenko formulation presented in relation (14).

The integral of Eq. 52 yields the nonlinear hysteretic stiffness matrix of the element:

$$[k_h] = EI \begin{bmatrix} -\mu_u & -\mu_u & 0 & 0 & 0 & 0 \\ 0 & 0 & -6\mu_\gamma & 6\mu_\gamma & -\mu_\phi/L & \mu_\phi/L \\ 0 & 0 & -3\mu_\gamma L & 3\mu_\gamma L & -\mu_\phi\left(1+6\lambda\right) & -6\mu_\phi\lambda \\ \mu_u & \mu_u & 0 & 0 & 0 & 0 \\ 0 & 0 & 6\mu_\gamma & -6\mu_\gamma & \mu_\phi/L & -\mu_\phi/L \\ 0 & 0 & -3\mu_\gamma L & 3\mu_\gamma L & 6\mu_\phi\lambda & \mu_\phi\left(1+6\lambda\right) \end{bmatrix} \tag{54}$$

where:

$$\begin{aligned}
\mu_u &= \left(1-\alpha_u\right)\frac{EA}{2EI} \\
\mu_\gamma &= \left(1-\alpha_\gamma\right)\mu \\
\mu_\phi &= \left(1-\alpha_\phi\right)\mu
\end{aligned} \tag{55}$$

Similarly to the elastic case, as λ tends to zero, μ tends to unity and the hysteretic matrix coincides with the one derived for the Euler–Bernoulli case [40]. Substituting the expressions derived back to the principle of virtual work (Eq. 50), the following constitutive equation is derived at the element level:

$$\{P\} = [k_e]\{d\} + [k_h]\{z\} = \left[[k_e]\ [k_h]\right]\left\{\tilde{d}\right\} \tag{56}$$

Eq. 56 together with the set of Bouc–Wen evolution equations defined either in relation (24) or relation (28) at $x = 0$ and $x = L$ smoothly describe the nonlinear cyclic response of a Timoshenko beam element. Considering for example relation (28), the corresponding nodal hysteretic quantities

are expressed as:

$$\begin{Bmatrix} \dot{z}_u \\ \dot{z}_\phi \\ \dot{z}_\gamma \end{Bmatrix}_{x=0,L} = \begin{Bmatrix} \dot{z}_u^{1,2} \\ \dot{z}_\phi^{1,2} \\ \dot{z}_\gamma^{1,2} \end{Bmatrix} = \begin{bmatrix} [I] - H_1 H_2 [R] & 0 \\ 0\ 0 & 0 \\ & \left(1 - H_1^s H_2^s\right) \end{bmatrix}_{x=0,L} \left[\bar{B}\right]_{x=0,L} \{d\} \tag{57}$$

where $\left[\bar{B}\right]$ is the strain displacement matrix introduced (15), properly reordered to account for the strain vector in relation (28).

4 Solution procedure

4.1 Standard second order formulation

For a specific plane frame structure with n_f degrees of freedom and given connectivity of n_{el} elements, mass distribution and boundary conditions, dynamic equilibrium can be established in terms of nodal displacements, velocities and accelerations as follows:

$$[M]_S \left\{\ddot{U}\right\} + [C]_S \left\{\dot{U}\right\} + [K]_S \{U\} + [H]_S \{Z\} = \{P(t)\} \tag{58}$$

where $[M]_S$, $[C]_S$, $[K]_S$ are the mass, viscous damping and stiffness square symmetric $(n_f x\ n_f)$ matrices respectively and $[H]_S$ is the orthogonal $\left(n_f\ x\ 6n_{el}\right)$ hysteretic matrix of the structure, while $\{P(t)\}$ is the $(nfx1)$ vector of external forces. Both $[K]_S$ and [H]$_S$ are assembled by their corresponding elemental contributions defined in Eq. 53 and 54 respectively, following the direct stiffness method, Bathe (2007). The mass matrix may correspond to a lumped mass diagonal matrix or a consistent mass matrix [4]. The viscous damping matrix in general may be of the form of a Rayleigh damping matrix [8].

The unknown vectors, namely the nodal displacement vector $\{U\}$ and the elemental hysteretic deformation vector $\{Z\}$, with dimensions $\left(n_f x 1\right)$ and $(6n_{el}x1)$ respectively, dictate the structure of the hysteretic matrix $[H]_S$. The hysteretic behaviour is defined at the element level in terms of hysteretic curvatures, centreline axial deformations and shear strains. The contribution of the hysteretic matrix of each element expressed in global terms is appended to form the corresponding hysteretic matrix $[H]_S$, which expresses the hysteretic contribution that corresponds to the total degrees of freedom of the structure. Equation 58, together with the evolution equations for the entire set of the introduced hysteretic parameters, fully describe the response of the system to a given external excitation and initial conditions.

The necessary modifications in a standard FEM code, so as to comply with the formulation presented herein mainly concern the evaluation of the hysteretic matrix $[H]_S$ and the establishment of the evolution equations. Moreover, the element proposed herein can be easily incorporated in a joined analysis–identification software, as proposed in [26]. Any type of integrator can be used to solve the system of nonlinear equations of motion such as the Newmark family of solvers. In this work, the Livermore family of solvers is used, [27], as described in the next Section.

4.2 State space formulation

By introducing as auxiliary unknown the vector of nodal velocities $\left\{\dot{U}\right\}$, the dynamic equilibrium Eq. 58 is expressed in the form of $2n_f$ linear differential equations of first order as follows:

$$\begin{Bmatrix} \left\{\dot{U}\right\} \\ \left\{\ddot{U}\right\} \end{Bmatrix} = [S] \begin{Bmatrix} \{U\} \\ \left\{\dot{U}\right\} \\ \{Z\} \end{Bmatrix} + \begin{Bmatrix} 0 \\ \{P(t)\} \end{Bmatrix} \tag{59}$$

where the state matrix [S] is defined as:

$$[S] = \begin{bmatrix} 0 & I & 0 \\ -[M]^{-1}[K] & -[M]^{-1}[C] & -[M]^{-1}[H] \end{bmatrix} \tag{60}$$

These are coupled with the nonlinear set of $6n_{el}$ evolution equations of the form:

$$\left\{\dot{Z}\right\} = f\left(\left\{\dot{U}\right\}, \{Z\}\right) \tag{61}$$

Equation 61 is formulated as 3 sets of pairs of coupled equations for each element defined in relations (57).

Equation 59 depends on global system matrices, which are defined once at the beginning of the analysis and remain constant in all subsequent steps. Moreover, the evolution of the elastoplastic behaviour is treated at the element level in a decoupled and thus implicitly parallel form considering an interaction scheme for the bending shear and axial components through relation (24) or the interaction of bending and axial components through relation (28).

Equation 59 are written into a non-autonomous state–space formulation of the following form:

$$\{\dot{x}\} = G\left(\{x\}\right)\{x\} + \{P\left(t\right)\} \tag{62}$$

where the vector $\{x\}$ is defined as:

$$\{x\}^T = \left[\{U\}^T \left\{\dot{U}\right\}^T \{Z\}^T\right] \tag{63}$$

and $G\left(\{x\}\right)$ is defined as follows:

$$G\left(\{x\}\right) = \begin{bmatrix} \mathbf{0} & I & \mathbf{0} \\ [M]^{-1}[K] & [M]^{-1}[K] & [M]^{-1}[H] \\ \mathbf{0} & Y\left(\left\{\dot{U}\right\}, \{Z\}\right) & \mathbf{0} \end{bmatrix} \tag{64}$$

The operator G is a state dependent operator since Y holds the evolution equations for each beam element i and beam

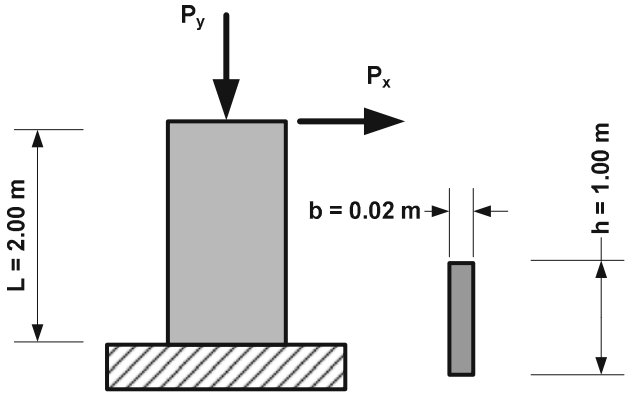

Fig. 3 Cantilever beam

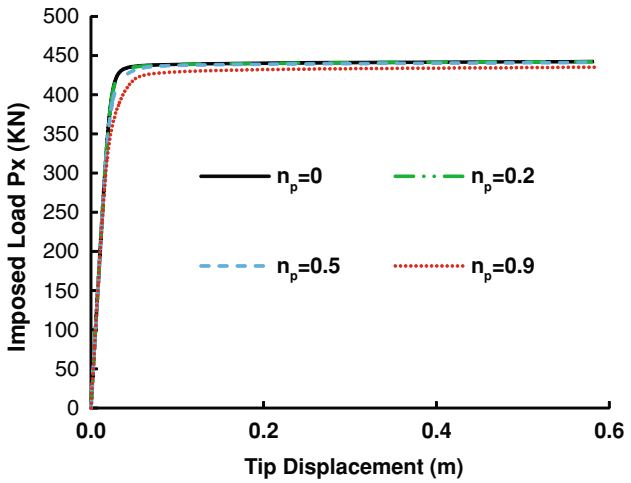

Fig. 4 Effect of the axial force on the bearing capacity of the element

end j, e.g. considering the interaction scheme of relation (28), vector Y is defined as:

$$Y_j^i\left(\{\dot{u}\}^i,\{z\}^i\right)=\begin{bmatrix}[I]-H_1H_2\,[R] & 0\\ 0\;0 & \left(1-H_1^sH_2^s\right)\end{bmatrix}_j\left[\bar{B}\right]_j\{\dot{d}\} \tag{65}$$

where $\{\dot{d}\}=[\Lambda]\,\{\dot{u}\}^i$ and $[\Lambda]$ is the transformation matrix of the 2D beam element from the global to the local coordinate system defined in equation.

$$[\Lambda]=\begin{bmatrix}\cos\psi & \sin\psi & 0\\ -\sin\psi & \cos\psi & 0\\ 0 & 0 & 1\end{bmatrix} \tag{66}$$

where ψ is the angle between the local x axis and the global x axis, as presented in Fig. 1.

5 Numerical verification

5.1 Example 1: cantilever beam

In this example, an aluminum cantilever beam presented in Fig. 3 is examined. At first, a horizontal load is applied at the tip and the elastic response of the cantilever is compared to the analytical solution to validate the behaviour of the element in terms of shear-locking. Next, a nonlinear static analysis is conducted and the load–tip deflection curve is plotted for different values of the vertical load $\mathrm{P_y}$.

For the nonlinear analysis, full interaction between axial, shear and bending is considered through relations (23) to (26). The yield criterion proposed by Simo et al. [33] is implemented:

$$\Phi=\left|\frac{M^h}{M_u^h}\right|+\left(\frac{N^h}{N_u^h}\right)^2\left(1+\left(\frac{V^h}{V_u^h}\right)^2\right)+\left(\frac{V^h}{V_u^h}\right)^4 \tag{67}$$

where for the rectangular cross-section $N_u^h=(1-\alpha_u)\,\sigma_y bh$, $V_u^h=\left(1-\alpha_\gamma\right)\sigma_y\big/\sqrt{3}bh$, $M_u^h=\left(1-\alpha_\phi\right)\sigma_y bh^2/4$, σ_y being the yield stress under uniaxial tension. The material properties considered are $E=69$ GPa, $G=26$ GPa, $\alpha_u=\alpha_\gamma=\alpha_\phi=0.0$, $n=25$, $\beta=\gamma=0.5$, $\sigma_y=275$ MPa. The shear coefficient for the rectangular cross-section is $k=5/6$. The tip horizontal displacement and the tip rotation are evaluated analytically as:

$$u_{x,exact}=\frac{\mathrm{P_x}L^3}{3EI}+\frac{\mathrm{P_x}L}{\beta GA}$$
$$\theta_{exact}=-\frac{\mathrm{P_x}L^2}{2EI}$$

Considering the stiffness matrix of the proposed beam element presented in relations (53) to (55) and under the assumption of elasticity, the tip displacement of the cantilever beam discretized into one element is evaluated as [41]:

$$\left.\begin{aligned}k_{55}^{el}u_x+k_{56}^{el}\theta=\mathrm{P_x}\\ k_{65}^{el}u_x+k_{66}^{el}\theta=0\end{aligned}\right\}\Rightarrow\begin{aligned}u_x&=\frac{\mathrm{P_x}L^3}{3EI}+\frac{\mathrm{P_x}L}{\beta GA}=u_{x,exact}\\ \theta&=-\frac{\mathrm{P_x}L^2}{2EI}=\theta_{exact}\end{aligned}$$

The formulation adopted yields an exact solution and no shear locking is developed, contrary to the Reduced Integration Timoshenko beam Element (RIE) and the Consistent Interpolation Beam Element (CIE) that both yield the following results [30]:

$$u_x^{RIE,CIE}=\frac{\mathrm{P_x}L^3}{4EI}+\frac{\mathrm{P_x}L}{\beta GA}\neq u_{x,exact}$$
$$\theta^{RIE,CIE}=-\frac{\mathrm{P_x}L^2}{2EI}=\theta_{exact}$$

in which, the rotation evaluated is exact but the translation is smaller.

Next, a monotonically increasing horizontal load $\mathrm{P_x}$ is imposed at the tip of the cantilever and a nonlinear static analysis is performed. In Fig. 4, the effect of the normalized

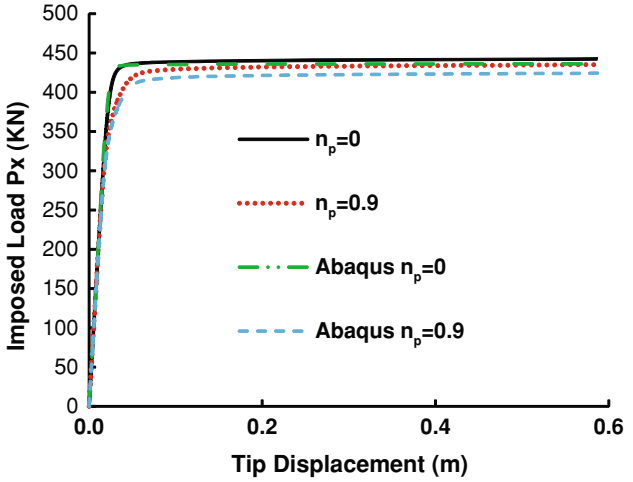

Fig. 5 Comparison of proposed formulation with plane stress solution

axial load $n_p = N^h/N_u^h$ on the nonlinear response of the cantilever is presented. The results obtained with the proposed formulation are compared with results obtained from Abaqus code [16]. In the latter, the cantilever is discretized with 160 quadrilateral plane stress elements considering a J_2 plasticity model, namely an elastic-perfectly plastic von-Mises material. Two cases are considered in Fig. 5 for $n_p = 0$ and $n_p = 0.9$ and the corresponding results from the proposed formulation and the Abaqus code are presented. Though in both cases, the ultimate load predicted by the proposed formulation is overestimated, the relative error is in both cases less than 1%. The ultimate load predicted from plasticity theory [18] for zero axial load is $P_U = \sigma_y bh^2/4L = 440KN$. The value predicted by the proposed formulation is $P_U = 440.8KN$, while Abaqus predicts a value of $P_U = 439.2KN$. The differences observed are due to the approximate nature of relation (67) as compared to the exact FEM solution. Nevertheless, the deviation of the proposed formulation from the exact solution for $n_p = 0.9$ is 2.6%. Moreover, the analysis with the proposed formulation completed in 1 sec, since only one beam element was used, while the analysis in the Abaqus code completed in 20 sec. All analyses were conducted in a PC fitted with a Pentium Core Duo processor and 4 GB of RAM.

5.2 Cyclically loaded shear beam

A 70 cm shear link of an IPE400 cross-section is examined in this paragraph. An S275 grade material is considered [2] with an elastic modulus of 210 GPa and a yield stress equal to 275 MPa. The solution obtained with the proposed formulation is compared against a solution obtained using Abaqus. The computational model implemented in the proposed formulation is presented in Fig. 6a. The structural

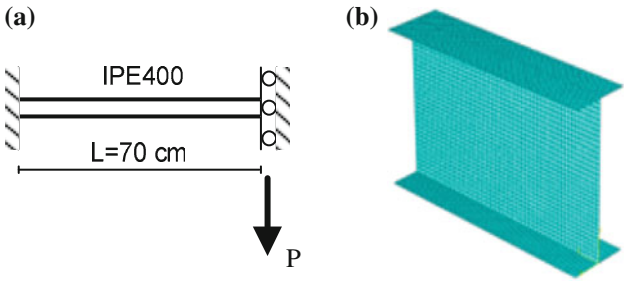

Fig. 6 **a** Idealized beam model. **b** Abaqus FEM mesh

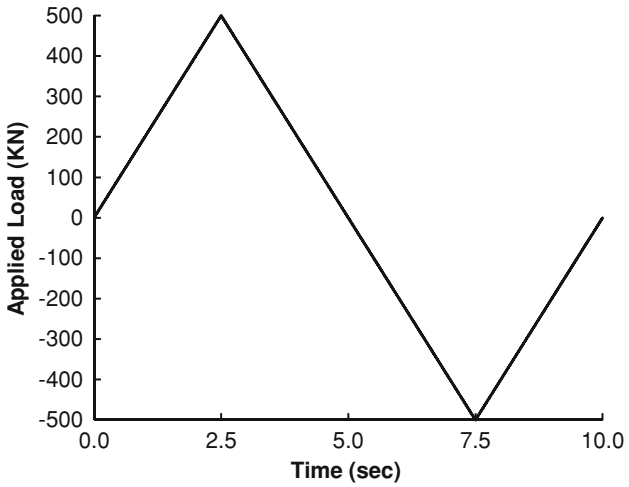

Fig. 7 Quasi-static loading

model implemented in Abaqus consists of 3712 quadrilateral shell elements and is presented in Fig. 6b. An elastic perfectly plastic material behaviour is considered in the Abaqus model. The parameters chosen for the Bouc–Wen model are $n = 6$, $\beta = \gamma = 0.5, \alpha_i = 0.025$. Due to the gradual yielding of the web, the elastic perfectly plastic stress-strain material law, attributed at the element level in the Abaqus discretization, gives rise to a hardening load-displacement path as presented in Fig. 8a, b. Therefore a nonzero kinematic hardening constant is assigned in the proposed macroelement to accurately simulate the actual behaviour.

The Orbison criterion is considered [23] defined by the following relation:

$$\Phi = 1.15n^2 + m_y^2 + m_z^4 + 3.67n^2m_y^2 + 3.0n^6m_z^2 + 4.65m_y^4m_z^2 \tag{68}$$

where $n = \frac{P^h}{P_u^h}$, $m_y = \frac{{M_y}^h}{M_{yu}^h}$, $m_z = \frac{{M_z}^h}{M_{zu}^h}$ while y refers to the strong axis and z refers to the weak axis of the cross-section. In this work, where only plane structures are considered m_z is equal to zero. Yielding in shear is defined by the following relation:

$${Q_y}^h = (1 - \alpha_\gamma)\frac{A_s\sigma_y}{\sqrt{3}} \tag{69}$$

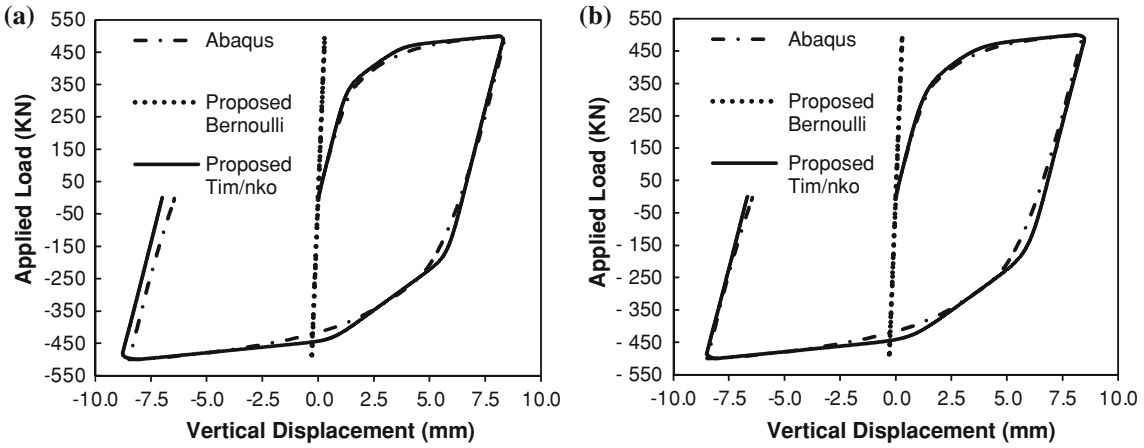

Fig. 8 **a** Force displacement curve, $n = 6$. **b** Force displacement curve, $n = 3$

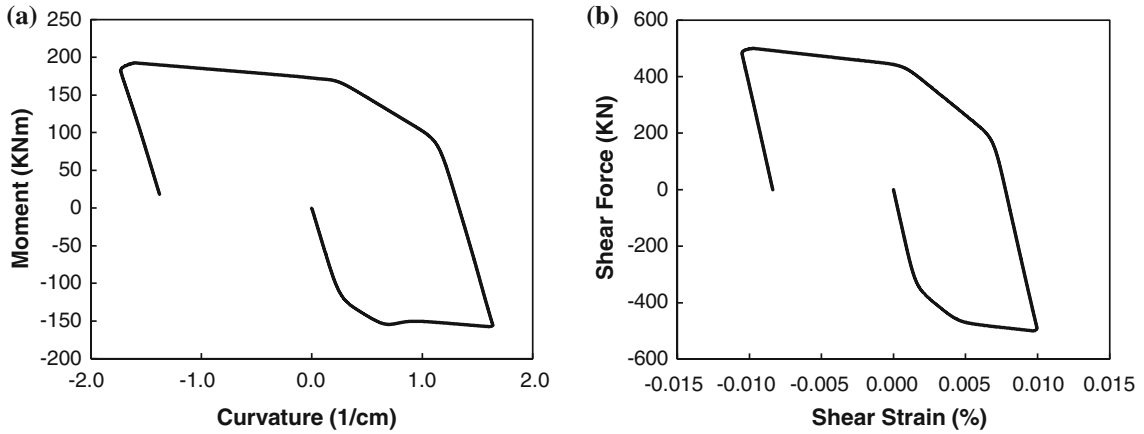

Fig. 9 **a** Moment–curvature diagram. **b** Shear force–Shear strain diagram

where A_s is the shear area of the cross-section and σ_y is the yield stress of the material under uniaxial tension. The plastic moment implemented into the Orbison criterion is considered a function of the shear force as defined by the following relation [14]:

$$M_{yu}^{h} = (1 - \alpha_\phi) M_p \left[1 - \frac{M_w}{M_p} \left(1 - \sqrt{1 - \left(\frac{Q}{Q_p} \right)^2} \right) \right]$$

where M_p is the plastic moment of a I section and M_w is the portion of bending retrieved from the web. A quasi-static analysis is performed under a cyclic excitation, presented in Fig. 7.

The response of the shear link is presented in Fig. 8a. Since the link yields in shear, the Bernoulli formulation fails to predict the nonlinear behaviour of the specimen. On the opposite, the Timoshenko formulation agrees well with the Abaqus results. The minor deviation both in the reloading phase and in the residual displacements is due to the inability of the proposed formulation to accurately predict the exact distribution of residual stresses on the cross-section that would give rise to a smoother transition from the elastic to the inelastic regime. However, allowing for a different set of parameters in the Bouc–Wen model, namely $n = 3$, $\beta = \gamma = 0.5$, $\alpha_i = 0.025$, the plot presented in Fig. 8b is produced.

The versatility of the implemented Bouc–Wen hysteretic rule on macro-modeling overcomes the inherent inability of the concentrated plasticity formulation to predict the smooth transition from the elastic to the inelastic regime due to the gradual yielding of the web. In Fig. 9a, b the moment–curvature and shear force–shear strain hysteresis loops are presented respectively. As concluded from the comparison of the Bernoulli and Timoshenko solutions, the shear link yields in shear since the ultimate moment asserted onto the element is less than the plastic moment of the IPE400 section (359 kNm).

5.3 Example 2: Woodland Hills Hospital—moment frame

In this example, a typical 6 story frame of a hospital building located at Woodland Hills, California is subjected to the El Centro accelerogram, scaled up with a factor of 1.8.

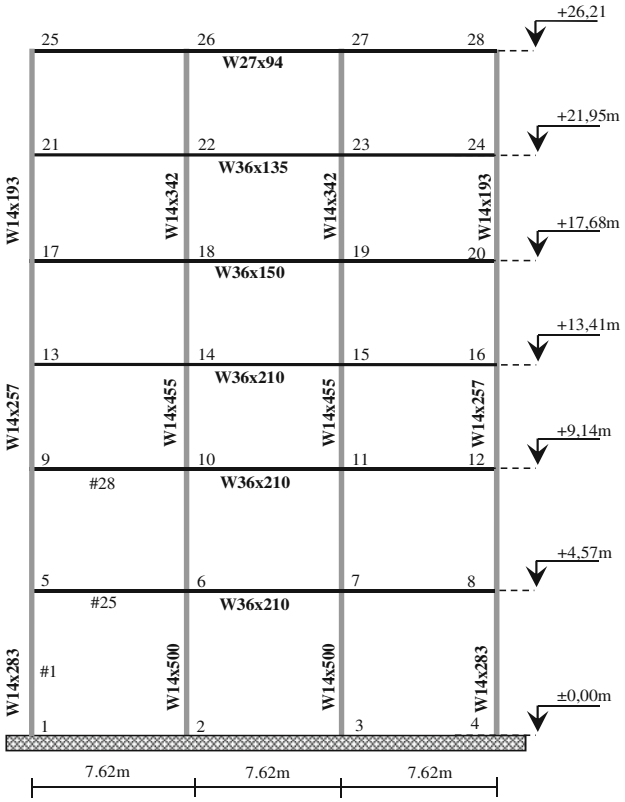

Fig. 10 Typical frame of Woodland Hills Hospital, California

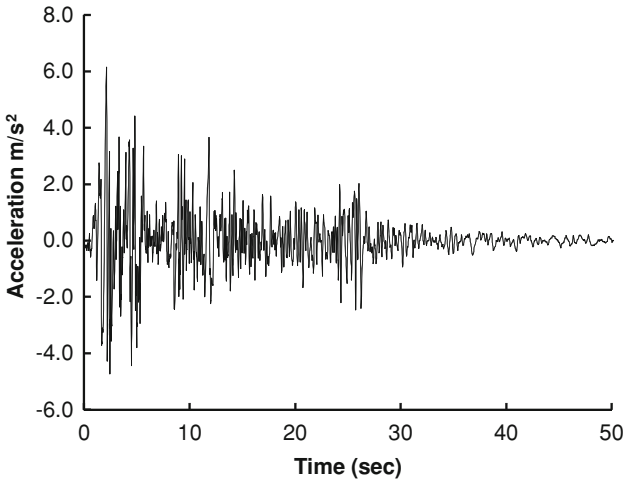

Fig. 11 Scaled El Centro ground motion record

The structure and the scaled accelerogram are presented in Figs. 10 and 11 respectively. Two analysis cases are considered.

In the first one the Euler–Bernoulli theory of bending is considered (setting $\lambda = 0$) and axial and bending plastic deformations are coupled through the Orbison criterion defined in Eq. 68. In the second, the Timoshenko formulation is used where yielding in shear is again defined by relation (69). The hysteretic axial, shear and moment resistance of the members are evaluated according to the cross-sectional data and presented in Table 1.

Table 1 Hysteretic member resistance

Cross-Section [−]	N_p $[KN]$	$Q_y{}^h$ $[KN]$	M_p $[kNm]$
W36×210	9,888	1,456	3,383
W36×150	7,063	1,040	2,360
W36×135	6,344	934	2,067
W27×94	4,436	653	1,129
W14×283	13,308	1,959	2,201
W14×257	12,093	1,781	1,977
W14×193	9,071	1,335	1,442
W14×500	23,494	3,458	4,262
W14×455	21,437	3,156	3,791
W14×342	16,158	2,379	2,726

Table 2 Material parameters

Parameter	Value
n	25
α_{col}	0.0015
α_{beam}	0.0015
β	0.5
γ	0.5
σ_y	248,200 kPa

To prove the validity of the proposed formulation, results obtained from the Euler–Bernoulli analysis are compared to results obtained from the OpenSees code [21]. The fiber force-based element [36] is implemented in OpenSees while plasticity is introduced into the element through a fiber approach, at integration points defined along the element's length. In this way, the interaction between axial and bending plastic deformations is accurately attributed, while plasticity in shear is considered uncoupled. For the sake of comparison, two models are considered in OpenSees, with three and ten integration points per member respectively. The modified Newton scheme is utilized with an average acceleration Newmark integrator. A uniaxial elastic-plastic material model with kinematic hardening is used in the OpenSees code with the hardening constant being equal to $H_kin = 45$GPa. This corresponds to a post-elastic to elastic stiffness ratio $a = 0.0015$. Viscous damping is not considered in both cases. The value of the shear correction factor is equal to 0.255 for all sections.

The parameters of the Bouc–Wen model and the floor masses are presented in Tables 2 and 3 respectively. The derived moment–curvature diagrams are bilinear with a sharp transition from the elastic to the inelastic regime. The mass of the structure is considered lumped at the floor levels.

Table 3 Floor Masses

Floor	Mass (tn)
1	402.8
2	231.2
3	180.4
4	180.4
5	180.4
6	182.1

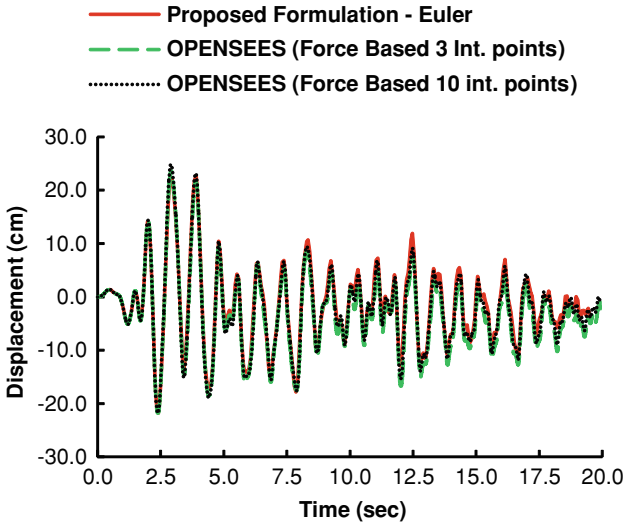

Fig. 12 Top story horizontal displacement time history (Euler Theory)

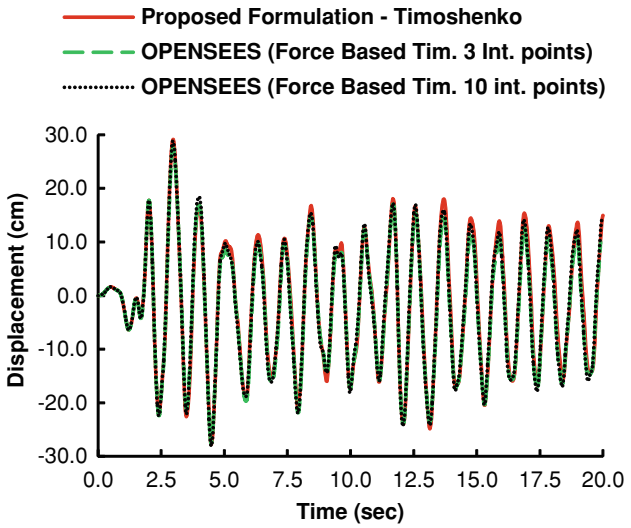

Fig. 13 Top story horizontal displacement time history (Timoshenko Theory)

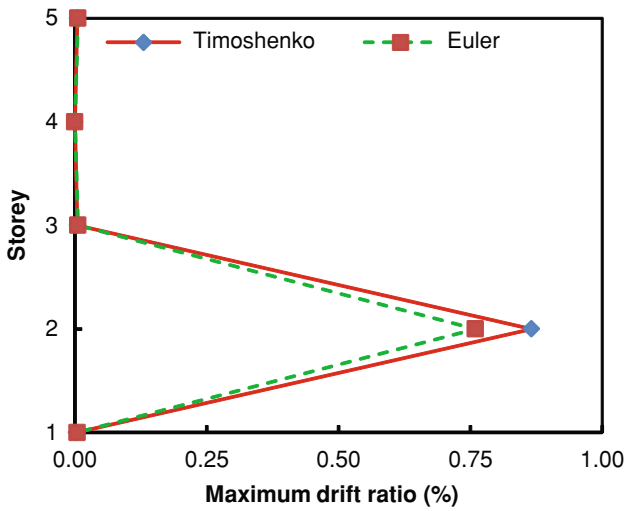

Fig. 14 Maximum drift ratios

The dynamic analysis is carried out for a time period of 20 seconds with a time integration step of 0.02 sec. The fundamental eigenperiod of the structure is $T_{Euler} = 0.94$ sec and $T_{TIM} = 1.05$ for the Euler and Timoshenko formulations respectively.

For the first analysis case, the time history of the top story horizontal displacement (node 28) is plotted in Fig. 12 where the results from OpenSees and the proposed formulation are compared. The results obtained from the proposed method and OpenSees are in perfect agreement. The minor differences observed are attributed to the different solution procedures implemented.

In the second analysis case, where the Timoshenko beam theory is considered, the dynamic response of the structure is considerably different. In Fig. 13, the time-history of the top-story horizontal displacement is again compared to the results obtained from OpenSees. The solution obtained from the proposed formulation agrees with the force-based scheme implemented in OpenSees.

As expected, the results obtained from the Euler–Bernoulli and Timoshenko formulation differ. In the first 4 seconds of the excitation the response of the structure is practically the same. However, as plastic deformations accumulate, both in bending and in shear, the flexibility of the structure is further increased. Thus, larger displacements are observed, especially towards the last 10 seconds of the response when plastic deformations accumulate, while the max and min response differ by 20–25%. In Fig. 14 the maximum interstorey drift ratios (IDRs) are presented for the two analysis cases. IDR is defined as the relative horizontal displacement of two subsequent storeys normalized to the storey height. It is concluded that the dynamics of the structure are not significantly altered considering either the Euler–Bernoulli or Timoshenko formulation, since the distribution of the maximum shear drifts remains the same. Plastic deformations in both cases are concentrated in the first storey columns. Thus, the differences observed between Figs. 12 and 13 are due to the shear plastic

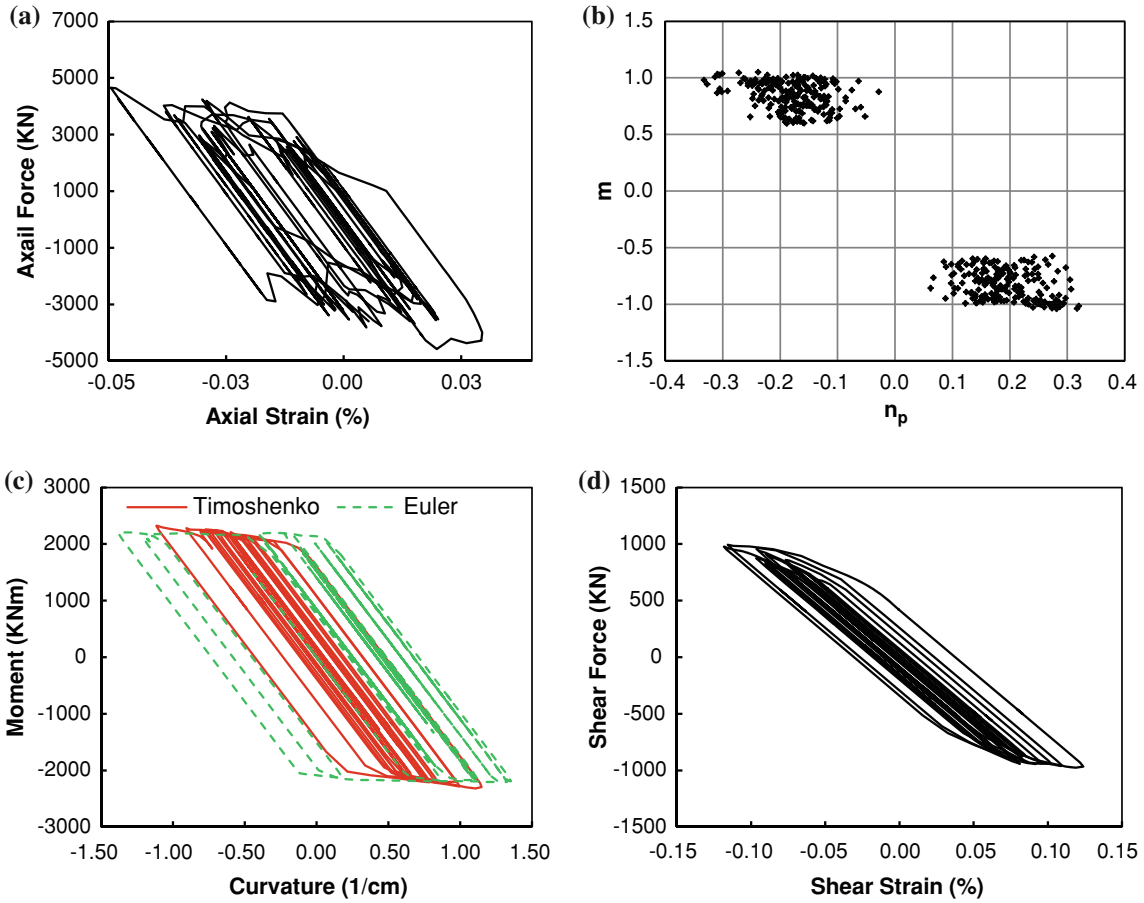

Fig. 15 **a** Axial force–axial deformation. **b** Normalized axial–moment dynamic interaction. **c** Moment–curvature. **d** Shear force–shear deformation

deformations being developed in the first storey-columns leading to a more flexible structure in the Timoshenko formulation.

In the next figures, the efficiency of the proposed hysteretic interaction scheme is presented. The axial force–axial deformation and moment–curvature diagrams of element #1 (Fig. 10) are presented in Fig. 15a, c respectively. In the latter, the moment–curvature hysteretic loop derived following Timoshenko formulation is compared against the Euler–Bernoulli formulation derived loop. Though the elastic stiffness of the member does not vary significantly, the maximum bending plastic deformations in the first case are smaller. In Fig. 15d the shear force–shear deformation hysteretic loop is plotted. Contrary to the Euler–Bernoulli case where energy is dissipated only through the hysteretic moment-curvature mechanism, in this case the shear hysteretic energy is also considered. Correct estimation of the actual section deformations is important in displacement based design where the capacity of a member is measured in terms of deformation potential.

In Fig. 15b, the normalized axial force and the normalized bending moment are plotted when yielding has occurred. These points foliate the corresponding space and do not lay on a single curve due to kinematic hardening. For the same reason normalized values exceed unity in the figure. As expected, yielding in bending is predominant in the nonlinear behaviour of the frame member. However, the interaction scheme significantly alters its plastic deformation potential.

A Fortran code has been developed for the analysis of skeletal structures with the proposed formulation. All the analyses were performed in a PC fitted with a Core Duo Quad CPU and 4 GBs of RAM. The analysis time with the proposed formulation was 67 sec. The analysis time of OpenSees was 118 sec for three integration points.

6 Conclusions

In this work, a new nonlinear beam element is presented, together with efficient methods for the solution of the equations of motion treating nonlinearities at the element level. The beam element is formulated within the framework of the Timoshenko beam theory by adding six new degrees of freedom accounting for the hysteretic part of the curvature,

axial centreline deformation and shear strain. Exact shape functions are utilized. As a consequence, shear locking is alleviated. The Bouc–Wen hysteretic model is implemented to simulate the nonlinear constitutive behaviour of the material. A wide range of hysteretic behaviour can be modeled by properly controlling the parameters of the hysteresis law, namely the "yield" parameter, the smoothness parameter n, and the shape factors, while existing extended models could be used to account for stiffness degradation, strength deterioration and pinching phenomena. The proposed element can be extended into 3D space in a concise and straightforward manner.

References

1. EN (1998) Eurocode 8 Earthquake, Part 3: Strengthening and repair of buildings
2. European structural steel standard (2004) EN 10025-2
3. Baber T, Noori MN (1985) Random vibration of degrading, pinching systems. J Eng Mech 111(8):1010–1026
4. Bathe KJ (2007) Finite Element Procedures. Prentice Hall Engineering, Science, Mathematics, New York
5. Bouc R (1967) Forced vibration of mechanical systems with hysteresis. In: Proceedings of the Fourth Conference on Non-linear oscillation. Prague, Czechoslovakia
6. Casciati F (1995) Stochastic dynamics of hysteretic media Lecture Notes in Physics 451. Springer, Berlin 270–283
7. Charalampakis AE, Koumousis VK (2008) Ultimate strength analysis of composite sections under biaxial bending and axial load. Adv Eng Softw 39(11):923–936
8. Chopra A (2006) Dynamics of structures. Prentice Hall Engineering, Science, Mathematics, New York
9. Dong SB, Alpdogan C, Taciroglu E (2010) Much ado about shear correction factors in Timoshenko beam theory. Int J Solids Struct 47:1651–1665. doi:10.1016/j.ijsolstr.2010.02.018
10. Foliente GC (1995) Hysteresis modeling of wood joints and structural systems. J Struct Eng 121(6):1013–1022
11. Friedman Z, Kosmatka JB (1993) An improved two-node Timoshenko beam finite element. Comput Struct 47(3):473–481
12. Guggenberger J, Grundmann H (2005) Stochastic response of large FEM models with hysteretic behaviour in beam elements. Comput Methods Appl Mech Eng 194:1739–1756
13. den Hartog JP (1999) Strength of materials. Dover, New York
14. Heyman J, Dutton WE (1954) Plastic design of plate girders with unstiffened webs. J Eng Weld Metal Fabric 22:265–272
15. Ismail M, Ikhouane F, Rodellar J (2009) The hysteresis Bouc-Wen model, a survey. Arch Comput Methods Eng 16:161–188
16. Karlsson Sorensenn, Hibbitt I (2000) Abaqus/standard user's manual, vol I, Version 6.1. HKS publications, New York
17. Kasai K, Popov EP (1986) General behavior of WF steel shear link beams. J Struct Eng 112(2):362–382. doi:10.1061/(ASCE)0733-9445(1986)112:2(362)
18. Lubliner J (2008) Plasticity theory. Dover, New York
19. Macneal RH (1978) A simple quadrilateral shell element. Comput Struct 8(2):175–183. doi:10.1016/0045-7949(78)90020-2
20. Mazza F, Mazza M (2010) Nonlinear analysis of spatial framed structures by a lumped plasticity model based on the Haar-Kàrmàn principle. Comput Mech 45:647–664
21. McKenna F, Fenves G, Scott M (2000) Open System for Earthquake Engineering Simulation. University of California, Available from: http://OpenSees.berkeley.edu
22. Neal BG (1961) Effect of shear force on the fully plastic moment of an I-beam. J Mech Eng Sci 3(2)
23. Orbison JG, McGuire W, Abel JF (1982) Yield surface applications in nonlinear steel frame analysis. Comput Methods Appl Mech Eng 33(1–3):557–573. doi:10.1016/0045-7825(82)90122-0
24. Ozdemir H (1976) Nonlinear transient dynamic analysis of yielding structures. Ph.D. dissertation, University of California, Berkeley
25. Papachristidis A, Fragiadakis M, Papadrakakis M (2010) A 3d fibre beam-column element with shear modelling for the inelastic analysis of steel structures. Comput Mech 45:553–572
26. Piyawat K, Pei JS (2009) Linking nonlinear system identification with nonlinear dynamic simulation under OpenSees(1213) Some justifications and implementations. J Eng Mech 135(11):1213–1226. doi:10.1061/(ASCE)0733-9399(2009)135:11
27. Radhakrishnan K, Hindmarsh AC (1993) Description and use of LSODE, the Livermore solver for ordinary differential equations. LLNL report UCRL-ID-113855
28. Rakowski J (1990) The interpretation of the shear locking in beam elements. Comput Struct 37(5):769–776. doi:10.1016/0045-7949(90)90106-C
29. Ramberg W, Osgood WR (1943) Description of stress-strain curves by three parameters. Technical Note No. 902, National Advisory Committee For Aeronautics, Washington DC
30. Reddy JN (1997) On locking-free shear deformable beam finite elements. Comput Methods Appl Mech Eng 149(1–4):113–132 (Containing papers presented at the Symposium on Advances in Computational Mechanics). doi:10.1016/S0045-7825(97)00075-3
31. Saidi M, Sozen MA (1979) Simple and complex models for nonlinear seismic response of concrete structures. In: Civil Engineering Studies SRS-465, Structural Research Series. University of Illinois Engineering Experiment Station. College of Engineering. University of Illinois at Urbana-Champaign
32. Saritas A, Filippou FC (2009) Inelastic axial-flexure-shear coupling in a mixed formulation beam finite element. Int J Non Linear Mech 44(8):913–922. doi:10.1016/j.ijnonlinmec.2009.06.007
33. Simo JC, Hjelmstad KD, Taylor RL (1984) Numerical formulations of elasto-viscoplastic response of beams accounting for the effect of shear. Comput Methods Appl Mech Eng 42(3):301–330. doi:10.1016/0045-7825(84)90011-2
34. Sivaselvan MV, Reinhorn AM (2000) Hysteretic models for deteriorating inelastic structures. J Eng Mech 126(6):633–640. doi:10.1061/(ASCE)0733-9399(2000)126:6(633)
35. Sivaselvan MV, Reinhorn AM (2003) Nonlinear analysis towards collapse simulation—a dynamic systems approach. Technical report, MCEER
36. Spacone E, Ciampi V, Filippou FC (1992) A beam element for seismic damage analysis. UCB/EERC-92/07, Earthquake Engineering Research Center, College of Engineering, University of California, Berkeley
37. Stolarski H, Belytschko T (1983) Shear and membrane locking in curved C0 elements. Comput Methods Appl Mech Eng 41(3):279–296. doi:10.1016/0045-7825(83)90010-5
38. Symeonov VK, Sivaselvan MV, Reinhorn AM (2000) Nonlinear analysis of structural frame systems by the state space approach. Comput Aided Civil Infrastruct Eng 15:76–89
39. Taylor RL, Filippou FC, Saritas A, Auricchio F (2003) A mixed finite element method for beam and frame problems. Comput Mech 31:192–203
40. Triantafyllou S, Koumousis V (2008) A beam element formulation for the nonlinear dynamic analysis of structures using the Bouc-Wen hysteretic rule. In: 6th GRACM International Congress on Computational Mechanics. Thessaloniki, Greece
41. Wang CM, Reddy JN, Lee KH (2000) Shear deformable beams and plates. Elsevier, New York
42. Wen Y (1976) Method of random vibration of hysteretic systems. J Eng Mech Div 102:249–263